

3D Arrangement of Magnetic Particles in Thin Polymer Films Assisted by Magnetically Patterned Exchange Bias Layer Systems

Iris Koch,* Markus Langner, Dennis Holzinger, Maximilian Merkel, Meike Reginka, Rico Huhnstock, Andreea Tomița, Claudia Jauregui Caballero, Andreas Greiner, and Arno Ehresmann*

The possibility to arrange and embed magnetic micro- and nanoparticles in thin polymer film systems using flat magnetically patterned substrate templates is investigated. In contrast to self-organized particle rows forming by applying a homogeneous magnetic field, particles adapt to the magnetic field landscape of the substrate's magnetic pattern prior to polymer crosslinking. Crosslinking then fixes the particle positions in the polymer. The process is tested for composites of hydrophobic polydimethylsiloxane (PDMS) and maghemite nanoparticles as well as for hydrophilic polyvinyl alcohol (PVOH) and hydrophilic functionalized, superparamagnetic core-shell microspheres. The substrate template is an exchange bias layer system magnetically patterned into parallel-stripe domains with in-plane magnetizations and head-to-head/tail-to-tail remanent magnetization orientation in adjacent magnetic domains. A high occupancy percentage of magnetic beads on a domain wall as well as anisotropic actuation of the composite is achieved.

1. Introduction

Magneto-sensitive elastomers (MSEs) are smart materials giving rise to innovative solutions for damping or insulating devices as well as sensors and actuators.^[1–5] Triggered by their


promising characteristics, these materials were already in focus of material research since the late 1980s and 1990s.^[1,2,6–8] MSEs usually consist of a polymer matrix with embedded magnetic micro- or nanoparticles (MPs). They exhibit magnetorheological as well as magnetostrictive effects, that is, the elasticity modulus and the lateral dimensions of the MSE can be reversibly set and controlled by external magnetic fields.^[1,6,9,10] Both effects are caused by dipolar interaction between the MPs and depend on their arrangement within the polymer matrix.^[8,9,11–13] Typically, MSEs with an anisotropic arrangement of MPs are formed by applying a magnetic field during the crosslinking of the polymer. In such cases, MP rows will form with lengths and average inter-row-distance depending on the MP concentration and

their magnetic characteristics.

Although the behavior of anisotropic MSEs is well-known in practice, their theoretical description is rather challenging. In most cases particle rows formed in three dimensions have been approximated by idealistic 2D arrangements of particle rows.^[13–15] 3D modeling requires considerably more computational effort aside from the usage of complicated analysis techniques, such as x-ray micro-computed tomography, in order to nondestructively examine the MPs' position in the MSE for the adaptation of the obtained model.^[16,17] Hence, elastomer matrices with true 2D particle arrays of rows with defined distances would be of tremendous advantage for further investigations on experimentally observed phenomena, comparison to theoretical work as well as for an enhanced controllability of the magneto-sensitivity.

In this work, we present a method to achieve a defined 1D and 2D positioning of MPs in a polymer matrix. Instead of solely using external magnetic fields for particle alignment which is usually associated with an imperfect particle row formation and nonuniform alignment of magnetic material,^[17–19] we propose a fabrication route employing a topographically flat magnetic template with designed domains for a defined magnetic field landscape (MFL) close to the substrate surface.^[20] We exemplify the method by using a template substrate covered by a magnetic thin film system with an engineered parallel-stripe

I. Koch, D. Holzinger, M. Merkel, M. Reginka, R. Huhnstock, A. Tomița, C. Jauregui Caballero, A. Ehresmann
Department of Physics and Center for Interdisciplinary Nanostructure Science and Technology (CINSaT)
University of Kassel
Heinrich-Plett-Straße 40, 34132 Kassel, Germany
E-mail: iris.d.koch@gmail.com; ehresmann@physik.uni-kassel.de
M. Langner, A. Greiner
University of Bayreuth
Macromolecular Chemistry
Universitätsstraße 30, 95440 Bayreuth, Germany

 The ORCID identification number(s) for the author(s) of this article can be found under <https://doi.org/10.1002/ppsc.202100072>.

© 2021 The Authors. Particle & Particle Systems Characterization published by Wiley-VCH GmbH. This is an open access article under the terms of the Creative Commons Attribution-NonCommercial-NoDerivs License, which permits use and distribution in any medium, provided the original work is properly cited, the use is non-commercial and no modifications or adaptations are made.

DOI: 10.1002/ppsc.202100072

domain pattern that extends over the surface of the entire template. Owing to the MFL, MPs of a still liquid polymer-MP mixture are attracted toward the substrate and aligned in defined geometric shapes during the hardening process.^[21,22] Thereby, MSEs with defined MP density gradients and anisotropies can be reproducibly created. The presented technique and prototype materials include hydrophilic and hydrophobic polymer matrices as well as ferrimagnetic iron oxide nanoparticles and superparamagnetic, chemically functionalizable core-shell microspheres. In addition, the surface material and thickness of the protecting capping layer above the magnetically patterned thin film system have been varied to analyze the applicability of different surface compositions for the alignment process.

2. Experimental Section

2.1. Materials

Two different types of polymer were used in the presented work: PVOH (hydrophilic) and PDMS (hydrophobic).

PVOH solution was purchased at SIGMA-ALDRICH Co. LLC. (87–89% hydrolyzed). PDMS base elastomer and curing agent were purchased at Biesterfeld Spezialchemie GmbH (Dow Corning Sylgard 184). Maghemite nanoparticles (g-Fe₂O₃, 20–40 nm, powder) were purchased at IOLITEC GmbH.

Superparamagnetic core-shell microspheres in aqueous solution (50 mg mL⁻¹) with a diameter of 2 μm were purchased at Micromod Partikeltechnologie GmbH. The spheres' cores consist of a polystyrene matrix surrounded by superparamagnetic magnetite particles (Fe₃O₄, 10–15 wt%). The shell is made of polyethylene glycol functionalized with carboxyl groups, thus being hydrophilic.

Target materials used for sputter deposition (Cu, Ir₁₇Mn₈₃, Co₇₀Fe₃₀, Ta, Au) of the exchange bias thin films were purchased at EVOCHEM Advanced Materials GmbH.

2.2. Fabrication of Magnetic Template

The magnetic template was made of a magnetically stripe patterned thin film system without topographic irregularities. To implement the thermally stable magnetic stripe domain pattern with independently specified magnetization orientations in individual domains, thin film systems revealing the exchange bias (EB) effect were used. The EB effect is manifested in a unidirectional magnetic anisotropy due to exchange interaction taking place at the common interface between a thin antiferromagnetic (AF) and a ferromagnetic (F) layer. The EB can be understood as an internal magnetic field that locally acts on the F's magnetic moments and impedes the magnetization reversal when an opposed external field is applied, that is, the F's hysteresis curve is shifted by the so-called EB field H_{eb} along the magnetic field axis. The EB bilayer system is typically embedded between a buffer layer for crystal texture improvement in the AF and a capping layer on top to prevent the F from oxidation.

For this work, the two different systems Cu^{50 nm}/Ir₁₇Mn₈₃^{10 nm}/Co₇₀Fe₃₀^{75 nm}/Ta^{15 nm} (A) and Cu^{50 nm}/Ir₁₇Mn₈₃^{10 nm}/Co₇₀Fe₃₀^{75 nm}/

Au^{10 nm} (B) were fabricated under high vacuum conditions via rf sputter deposition (Leybold-Heraeus Z400) on a naturally oxidized silicon substrate (15 × 15 mm²). The EB effect was initialized by a field cooling process, that is, heating of the sample in an external magnetic field ($H_{FC} = 100 \text{ kA m}^{-1}$) up to 300 °C (plateau: 1 h) and subsequent cooling down to room temperature. In order to create the parallel magnetic stripe domains out of the uniformly magnetized EB system, a process termed ion bombardment induced magnetic patterning (IBMP) was performed.^[20,23,24] In this process, a widened helium ion beam is used in combination with a polymer-based shadow mask in an applied external magnetic field to locally modify the strength and direction of the EB, that is, to create magnetic domains. Therefore, a 700 nm thick resist layer (positive resist AZ 1505, purchased at Microchemicals GmbH) was spin coated on top of the EB substrates and subsequently irradiated by UV-light (Hg lamp) through a chromium hard mask (shadow mask), resulting in parallel stripe structures of photoresist with 5 μm (10 μm periodicity) and 10 μm stripe width (20 μm periodicity), respectively after development in 0.9% KOH solution. This process was followed by 10 keV He⁺ ion bombardment in an external magnetic field ($H_{IB} = 80 \text{ kA m}^{-1}$) under high vacuum condition. Thereby, the in-plane magnetization direction was only altered in the resist-free areas due to ion penetration and, thereby, local hyperthermal heating of the layer system. With the external magnetic field direction being antiparallel and the long axes of the resist stripes being perpendicular to the initial EB direction, a head-to-head and tail-to-tail configuration (hh/tt) of the magnetization direction in adjacent magnetic domains was generated. Subsequently, the remaining resist stripes were removed via oxygen plasma etching resulting in topographically flat EB sample surfaces with typical RMS roughness values of (0.6 ± 0.4) nm. A depiction of the fabrication process is shown in **Figure 1**.

After each fabrication step, the EB substrates were characterized by vibrating sample magnetometry (VSM, see **Figure 2a**), where they exhibited a shift of the hysteresis loop along the magnetic field direction with average EB fields of $H_{eb,A} = (-21.3 \pm 1.7) \text{ kA m}^{-1}$ and $H_{eb,B} = (-24.8 \pm 0.5) \text{ kA m}^{-1}$ and average coercive fields of $H_{c,A} = (9.8 \pm 0.7) \text{ kA m}^{-1}$ and $H_{c,B} = (4.4 \pm 0.1) \text{ kA m}^{-1}$, that is, the samples have one stable magnetization direction in the absence of an external magnetic field.

The VSM measurements after He⁺ ion bombardment and removal of the photoresist showed characteristic double hysteresis loops for the bombarded samples (compare **Figure 2a**) and, thereby, indicated that the samples possess two well-defined remanent magnetization states. Magnetic force microscopy analysis of the EB samples displayed alternating magnetic line-shaped signals corresponding to the respective domain wall type (see **Figure 2b,c**), here exemplarily shown for 5 μm parallel stripe width.

2.3. Fabrication of Particle Polymer Composites on Magnetically Patterned EB Systems

The PDMS matrices were fabricated by mixing of the base and the curing agent at a mass ratio of 10:1. The liquid polymer was then degassed under vacuum in a desiccator. PVOH was prepared via mixing of a 10% PVOH solution and distilled water at a ratio

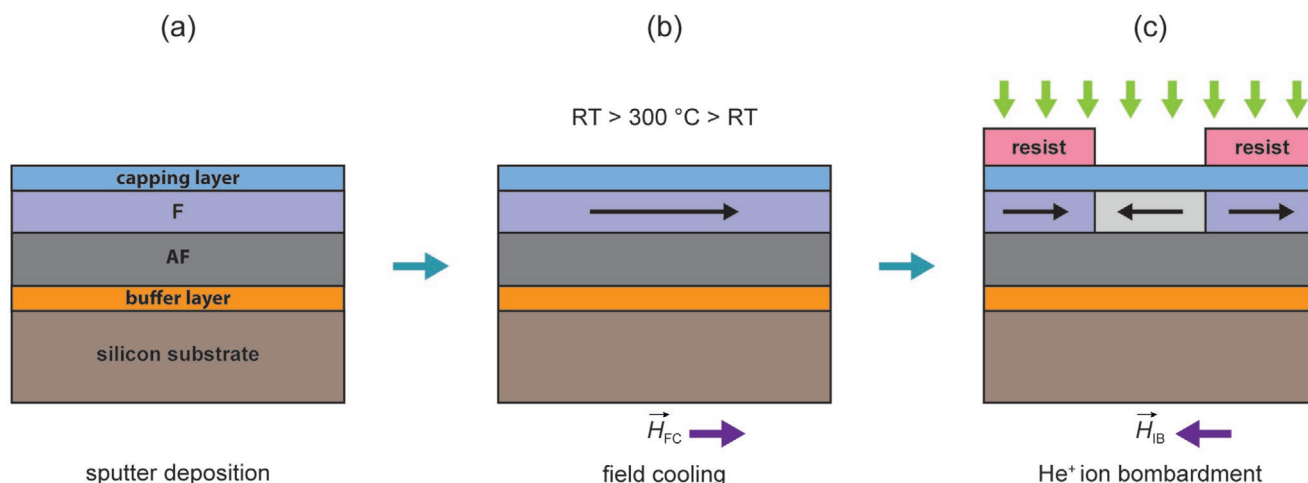


Figure 1. Fabrication of a magnetically patterned exchange bias system via ion bombardment: The exchange bias system consisting of an antiferromagnetic (AF) and a ferromagnetic (F) layer is fabricated via sputter deposition on top of a silicon substrate and covered with a capping layer for oxidation protection (a). The following field cooling process in an external magnetic field H_{FC} induces a unidirectional anisotropy parallel to the external magnetic field direction (b). Micromagnetic patterning of the exchange bias substrates is achieved by He^+ ion bombardment in an external magnetic field H_{IB} antiparallel to H_{FC} through a resist mask created via UV lithography (c). Afterward, the resist is removed and topographically flat sample surfaces are obtained.

of 1:1. The mixture was homogenized in a shaker for 10 min and subsequently allowed to rest for 60 min in order to remove air inclusions. Magnetic material was added to the polymer solutions before the degassing step. In detail, composite 1 consisted of hydrophobic PDMS and maghemite particles (3.1 wt%), while composite 2 was composed of a hydrophilic PVOH matrix with superparamagnetic, carboxyl-functionalized microspheres (0.33 wt%). Each polymer composite was subsequently cured on top of an EB system at room temperature for 24 h.

In order to prevent the thin film system from being peeled off while removing the polymer films due to the strong adhesive forces between the PDMS (PVOH) and the metallic surface, an additional resist layer (AZ 1505, 700 nm) was first spin coated on top of the magnetically stripe patterned EB

systems. The positioning of the magnetic material was supported by an additional magnetic field in z -direction parallel to the substrates' surface normal (Nd permanent magnet, 20 mm diameter, 200 mT at the surface). The composite films were finally obtained via a lift-off process in an acetone bath, where the resist layer was immediately dissolved. Afterward, the particle polymer composites were rinsed with distilled water and dried in a nitrogen stream.

3. Results and Discussion

In the present work, the general idea of using a magnetically patterned flat substrate as a template for MP positioning

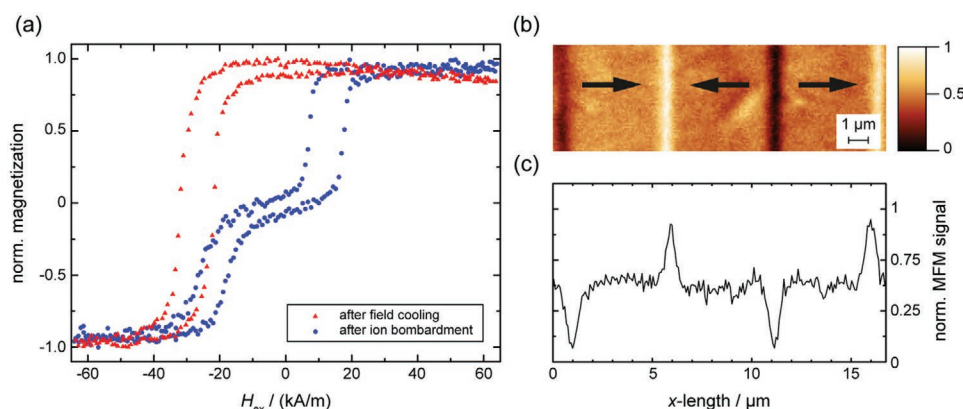


Figure 2. Magnetic characterization of the utilized exchange bias systems via VSM and MFM exemplarily shown for a sample of system type B: a) Typical hysteresis loops of the used exchange bias system prior to (red triangles) and after ion bombardment (blue dots) measured with VSM. After the field cooling process, the exchange-coupled antiferromagnet/ferromagnet system exhibits a defined magnetization direction in the absence of an external magnetic field. The ion bombardment induced magnetic patterning into a parallel stripe structure with antiparallel magnetization directions in adjacent domains leads to a characteristic double hysteresis loop. b) The additional analysis of the magnetically patterned exchange bias systems with MFM reveals alternating head-to-head (white signal) and tail-to-tail (black signal) domain wall types with distances depending on the utilized stripe periodicity (here: 5 μm stripes, i.e., 10 μm periodicity). The corresponding cut line profile of the normalized MFM signal is shown in (c).

is realized by a magnetically patterned exchange bias layer system. Here, past work has shown that engineered head-to-head and tail-to-tail (hh/tt) parallel-stripe domains of the magnetic template result in neighboring domain walls carrying opposite magnetostatic charges.^[25,26] Therefore, a grating-like arrangement of localized stray field sources possessing stray field strengths of up to 1 kA m^{-1} at distances of 1000 nm from the surface are created.^[26–28] As a result of the comparably strong local field gradients of up to several hundred MA m^{-2} ,^[27] attractive magnetostatic forces are acting on the MPs in the as yet not hardened polymer matrix. For superparamagnetic particles, these stray fields lead to an alignment of the particles' magnetic moments along the local magnetic field lines and a positioning of the particles above each domain wall of the substrate, as these are the regions where the stray field's strength and gradient are maximized. As the effective field for the current template is strongest over the center of the domain wall and perpendicular to the substrate surface, the magnetic moments of the superparamagnetic particles residing on one domain wall are parallel to each other.

Due to the parallel alignment of the neighboring particles' magnetic moment within each domain wall, magnetostatic repulsion largely prevents from lateral clustering. Besides, the agglomeration of particles perpendicular to the template surface is also mostly suppressed due to the energy gain when the particles approach the template surface. By superimposing the template's periodic stray field landscape with an external

field perpendicular to the template surface, the particles' magnetic potential energy landscape is modified by the alternating constructive and destructive superposition between the local field directions (see **Figure 3**) and the external field. As a result, those domain wall positions above which the local stray field is parallel to the external field are energetically favored. This leads to a rearrangement of the particle rows where every second domain wall of the magnetic stripe patterned template is occupied resulting in a doubling of the pattern's lattice distance.^[28]

The MP arrangement without an external field was found to be also working, but less efficiently due to the smaller magnetic force on the particles, which is proportional to the product of the magnetic field strength and field gradient. This can be explained by the comparably weak acting fields which do not magnetically saturate the particles. The stronger effective magnetic field caused by the superposition of the template's intrinsic magnetic field landscape and the external magnetic field induces higher magnetic moments in the particles and therefore leads to higher magnetic forces.

To make sure that the magnetic material is homogeneously distributed in the polymer matrix without agglomeration prior to sedimentation and polymer hardening, the prototype polymer materials used for fabrication of the composites were adapted to the material of the MPs, that is, hydrophobic polydimethylsiloxane (PDMS) was mixed with maghemite nanoparticle (MNP) powder (type 1), whereas hydrophilic polyvinyl alcohol (PVOH) was mixed with hydrophilic superparamagnetic core-shell

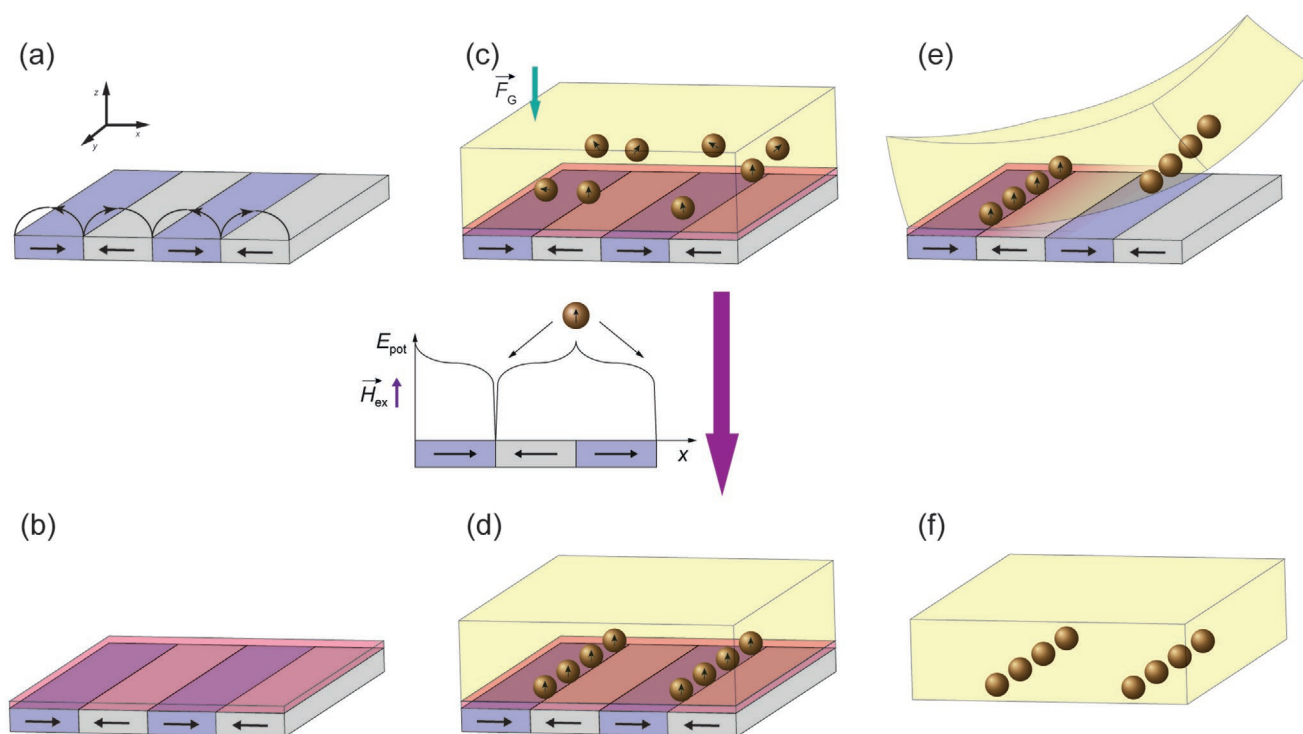


Figure 3. Fabrication of polymer films with embedded magnetic particles. a) Magnetic template with parallel-stripe domains fabricated by ion bombardment induced magnetic patterning (IBMP)^[20] of an exchange-bias bilayer system. b) Capping of the magnetic template by a 700 nm thick photoresist layer to prevent the magnetic layer system from being peeled off. c) Liquid polymer containing the (superpara)magnetic particles is poured over the magnetic template. Particles sediment to the bottom due to gravity \vec{F}_G . d) By superimposing an external magnetic field \vec{H}_{ex} perpendicular to the substrate surface, the particles are attracted to every second domain wall, forming equidistant, parallel rows. Finally, the hardened particle polymer film is removed after curing by an acetone-mediated lift-off (e,f).

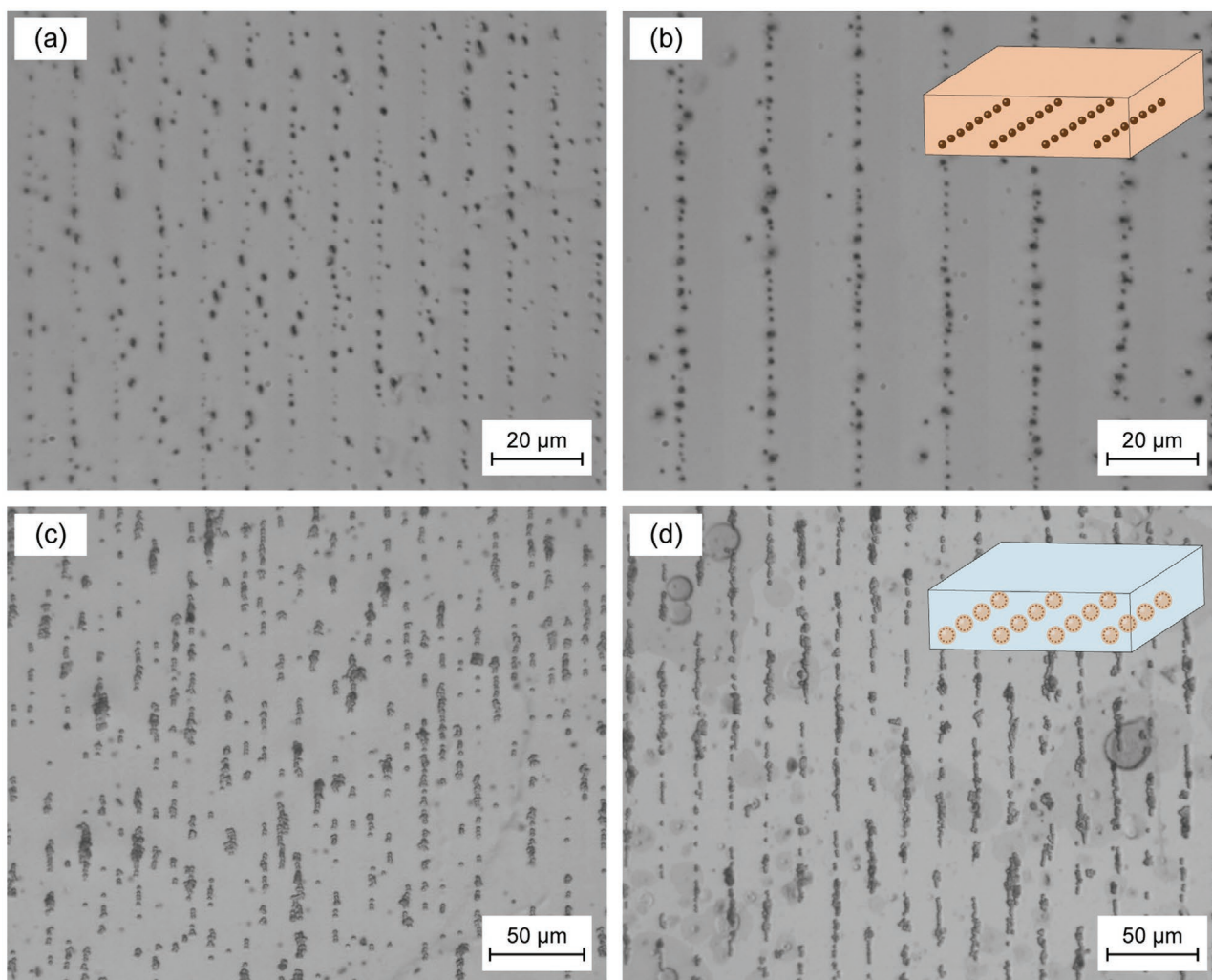


Figure 4. Optical microscopy images of particle polymer composite films: a,b): Maghemite nanoparticles embedded into a 70 μm thick PDMS film. The particles were arranged on top of exchange bias system type A (15 nm tantalum capping layer) with 5 μm (a) and 10 μm (b) domain width. Due to an additional external magnetic field applied during the curing of the particle polymer composite, the magnetic particles align in 10 and 20 μm distance, respectively. c,d): Superparamagnetic core-shell microspheres (2 μm diameter) embedded in 40 μm thick PVOH films. In order to align the microspheres, exchange bias systems of type B (10 nm gold capping layer) with 5 μm (c) and 10 μm (d) stripe domain width were used. Again, an external magnetic field was applied perpendicular to the substrate surface during curing.

microspheres (SCM, type 2). As PDMS is easy to handle and—regarding probable future applications—biocompatible, it is often the material of choice for magneto-sensitive elastomers.^[5] PVOH, on the other hand, is water-soluble and might therefore be interesting for applications where a localized release of magnetic material is required.

The present polymer films deposited by drop-coating exhibit thicknesses of 70 μm for composite type 1 and 40 μm for composite type 2 with magnetic material located at the polymer film's interface facing the magnetic template. The arrangement of the particles in the hardened polymer films was characterized via optical microscopy (see **Figure 4**).

The number of MPs was estimated for small MP densities between the domain walls. Positioning of MPs into parallel rows with distances corresponding to the doubled domain width of the respective magnetically patterned sample was observed for two different capping layers (Ta 15 nm and Au

10 nm), thus indicating that the material as well as its thickness does not influence the positioning as long as the magnetic stray fields are sufficiently strong to attract the MPs above the protective layer. Furthermore, it was proven that the positioning worked for two different widths (5 and 10 μm) of the magnetic parallel-stripe domains.

The average occupancy percentage ($100 \times (\text{average number of particles} \times \text{particle diameter}) / \text{domain wall length}$) of the rows in **Figure 4a–d** have been determined by counting the particles along a row. The identification of the MPs in the microscopic images has been carried out by defining a threshold contrast for the distinction between particles and background. Occupancy percentages of $(40 \pm 4)\%$ resp. $(55 \pm 7)\%$ (**Figure 4a** resp. **Figure 4b**) and $(39 \pm 8)\%$ resp. $(55 \pm 10)\%$ (**Figure 4c** resp. **Figure 4d**) have been determined. The occupancy percentages of both materials are equal within the uncertainties for equal stripe domain widths. Further analyzing the quality

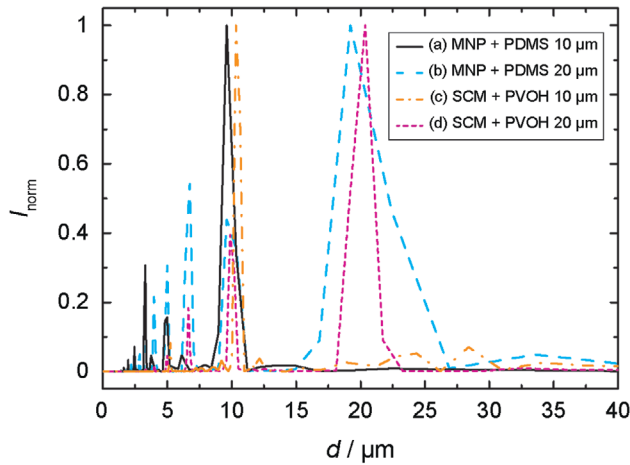


Figure 5. Power spectral density for the corresponding images shown in Figure 2a (black solid, MNP in PDMS, 10 μm periodicity), 2b (blue wider dashed, MNP in PDMS, 20 μm periodicity), 2c (orange dash-dotted, SCM in PVOH, 10 μm periodicity), and 2d (magenta small dashed, SCM in PVOH, 20 μm periodicity) normalized to the respective maximum intensity value I_{norm} . The position d characterizes the real-space coordinate in x -direction.

of arrangement by using the power spectral density function (PSDF), that is, performing a Fourier transformation of the autocorrelation function, of Figure 4a–d results in the graphs shown in **Figure 5**. For Figure 4a, the dominant peak is at $d = 9.6 \mu\text{m}$ with small contributions at $5.0 \mu\text{m}$ (beads still residing on the domain wall with antiparallel directions of the external and domain wall fields) and at about $3.3 \mu\text{m}$ (MP agglomerates and MPs not attracted to the domain walls). A similar result (main peaks appear at $d = 5.2$ and $10.3 \mu\text{m}$) is shown for Figure 4c for the same magnetic template pattern periodicity but for a different polymer. For the wider pattern periodicity, Figure 4b,d exhibits dominant peaks at $19.4 \mu\text{m}$ ($20.4 \mu\text{m}$) and a smaller peak at $9.6 \mu\text{m}$ ($9.9 \mu\text{m}$), indicating particles predominantly residing over the energetically favored domain wall and with less probability over the unfavored walls. Small peaks at other periodicities are attributed to MP agglomerates and MPs not residing above a domain wall.

A possible magnetostrictive effect is estimated by the following assumptions: 1) The external magnetic field is homogeneous and induces a fixed magnetic moment in the MPs. 2) The particles' magnetic moments are point dipoles located at their centers. 3) The interaction between two adjacent particles is described by the magnetic dipole–dipole interaction energy E_{dip} . The two particles shall have equal magnetic moments $\vec{m}_1 = \vec{m}_2 = \vec{m}$ and are located at a particle-to-particle-center distance \vec{r} . In general, their magnetic moments may have individual angles with respect to \vec{r} . For superparamagnetic particles in an external magnetic field, however, these two angles are the same and will now be designated as β (see **Figure 6a**). The interaction energy is then given by

$$E_{\text{dip}}(|\vec{r}|) = \frac{\mu_0}{4\pi} \left(\frac{|\vec{m}|^2}{|\vec{r}|^3} - 3 \frac{(|\vec{m}||\vec{r}| \cos(\beta))^2}{|\vec{r}|^5} \right) \quad (1)$$

where in the first term on the right hand side of Equation (1), the angle between the two individual magnetic moment directions has been set to 0° (see **Figure 6a**).

The magnetostatic forces between particles in one of the rows induced by an external field after removal of the polymer film from the magnetic template are calculated according to $\vec{F}_M = -\nabla E_{\text{dip}}$. Depending on β and the interparticle distance vector \vec{r} , the magnetostatic force can be derived from Equation (1) to

$$\vec{F}_M = \frac{3\mu_0}{4\pi} \cdot (1 - 3\cos^2\beta) \cdot \frac{|\vec{m}|^2}{(r_x^2 + r_y^2 + r_z^2)^2} \quad (2)$$

with the individual components of \vec{r} setting r_x as the distance along the short stripe axis of the magnetic pattern, that is, between separate particle rows, r_y as the distance along the long stripe axis of the magnetic pattern, that is, within one particle row, and r_z as the relative center particle height difference between adjacent particles. When particles have been integrated into the polymer after sedimentation to the magnetic template surface, r_z becomes zero (particles are at the same height), modifying Equation (2) to:

$$\vec{F}_M = \frac{3\mu_0}{4\pi} \cdot (1 - 3\cos^2\beta) \cdot \frac{|\vec{m}|^2}{(r_x^2 + r_y^2)^2} \quad (3)$$

From **Figure 6** it is evident that

$$\beta = \beta_0 - \gamma \quad (4)$$

where β_0 is the angle between the external magnetic field direction \vec{H} (or the particles' magnetic moment \vec{m}) and r_x and γ is the angle between \vec{r} and the x -axis with

$$\gamma = \tan^{-1} \left(\frac{r_y}{r_x} \right) \quad (5)$$

Considering only the directly neighboring particles in adjacent rows, that is, $r_y = r_z = 0$, Equation (3) can be further simplified to

$$F_{M,x} = -\frac{\partial E}{\partial r_x} = \frac{3\mu_0}{4\pi} \cdot (1 - 3\cos^2\beta) \cdot \frac{|\vec{m}|^2}{r_x^4} \quad (6)$$

with $\beta = \beta_0$. The term $(1 - 3\cos^2\beta)$ already suggests that there will be a change of sign in the force values at an angle of $\beta = 54.7^\circ$ between external magnetic field direction and distance vector \vec{r} and therefore a switching between an attractive and a repulsive state is possible.

Figure 6b shows the values of $F_{M,x}$ calculated for the used maghemite nanoparticles for different distances $|\vec{r}| = r_x$ between single particles and varying angles β_0 with $|\vec{m}| = 2.36 \times 10^{-12} \text{ Am}^2$ based on a prototypical spherical agglomerate of 45 spherical particles with a diameter of $d_p = 30 \text{ nm}$ each consisting of maghemite molecules with a magnetic moment of $\mu = 5\mu_B$.^[29] As the widths of the domain walls of the magnetically patterned substrate are at least one order of magnitude larger than the particle diameters, the particles

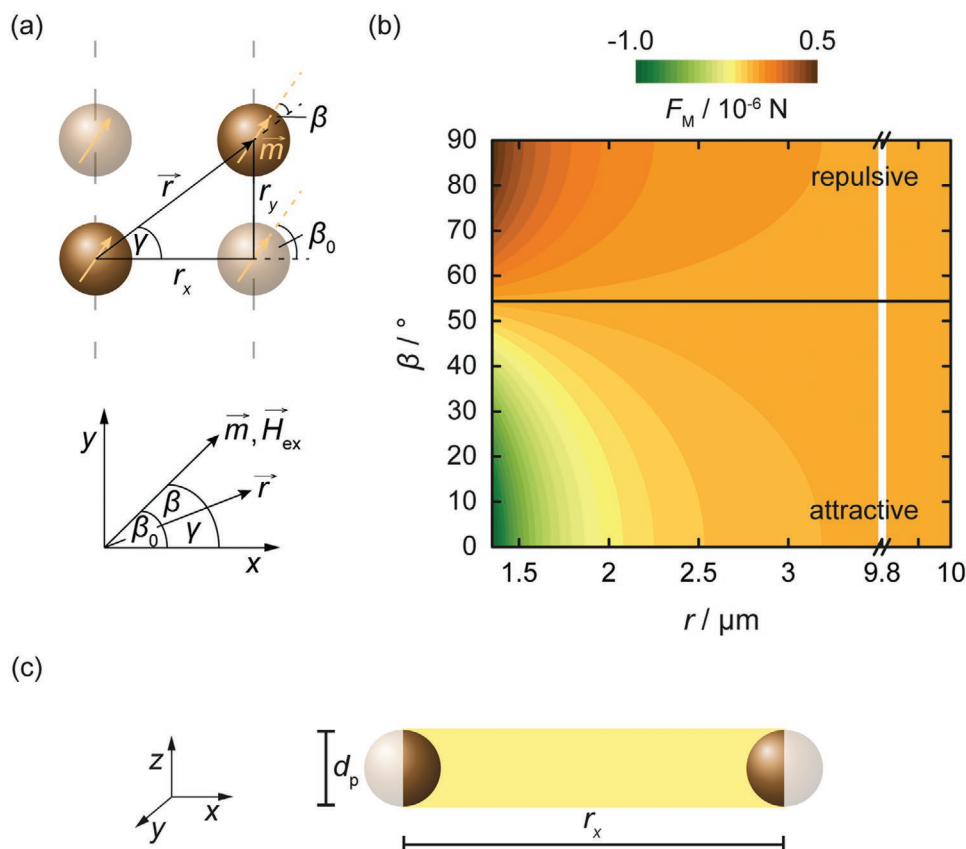


Figure 6. a) Sketch of the relevant angles and distances between neighboring particles for $r_z = 0$: The distance between two particle centers can be expressed by the distance vector \vec{r} . Particles with magnetic moment \vec{m} within one row (dashed gray line) are separated by a distance r_y , whereas particles in neighboring rows are additionally separated by the r_x component of \vec{r} . The angle β is defined as the angle between \vec{r} and \vec{m} (resp. \vec{H}_{ex} , as particles are assumed to be saturated by the external magnetic field). It is varied with changing angle γ or r_y , respectively. Note that the sum of β and γ is equal to the initial angle β_0 between \vec{r} and \vec{m} for $r_y = 0$. b) Magnetostatic force \vec{F}_M between magnetic particles depending on the angle β_0 between the particle-to-particle center distance vector \vec{r} and the external magnetic field induced magnetization \vec{m} and the interparticle distance r_x exemplarily shown for $r_y = 0 \text{ nm}$. The black line indicates the transition angle β_0 at which the interaction switches from attraction to repulsion. The values are calculated for agglomerates consisting of 45 maghemite nanoparticles. c) Sketch of a cylindrical polymer unit cell including magnetic particles with diameter d_p and length r_x .

build agglomerates and, thereby, exhibit stronger forces in reality as compared to the model. Considering two directly neighboring particle agglomerates with a minimum interparticle distance of $r = 1.35 \mu\text{m}$, the obtained maximum values of the magnetostatic force \vec{F}_M are in the order of 10^{-6} N . In contrast, two MNPs located at neighboring particle rows of $10 \mu\text{m}$ distance—as it was set in the experiments—experience a magnetostatic force in the range of 10^{-10} N . Therefore, the anisotropic distribution of magnetic material also leads to an anisotropic force distribution within the polymer film when applying an external magnetic field.

If $r_y \neq 0$, the angle γ between the x -axis and the distance vector \vec{r} has to be considered (see Figure 6a). Note that β changes with $\gamma \neq 0$ (see Equations (4) and (5)).

The angle β_0 at which the sign change of the force values \vec{F}_M , that is, the switching between attractive and repulsive magnetostatic interaction occurs is no longer constant, but depends on the ratio between r_y and r_x :

$$\beta_0(r_x, r_y) = \tan^{-1}\left(\frac{r_y}{r_x}\right) + \cos^{-1}\left(\frac{1}{\sqrt{3}}\right) \quad (7)$$

Based on that exact knowledge of the angular dependence of $\vec{F}_M(\vec{H})$ and $\vec{m}(\vec{H})$ in combination with the defined alignment of the particles in the polymer matrix, an application-adapted usage of the composite film is possible. As the results shown in Figure 6b are solely based on the present experimental conditions, magnetostatic forces that are several orders of magnitudes larger should be achievable by using reduced domain widths of the template^[30,31] or magnetic materials with larger magnetic moment, for example, $\text{Co}_{40}\text{Fe}_{60}$.^[32]

The elastic energy U_{ela} of a hyperelastic medium that is assumed to be fixed in the z -direction with elastic modulus E_{sample} and volume V_{sample} is described by the Neo–Hooke law^[31]

$$U_{\text{ela}} = \frac{E_{\text{sample}}}{6} \cdot \left((1 + \epsilon)^2 + \frac{1}{(1 + \epsilon)^2} - 2 \right) \cdot V_{\text{sample}} \quad (8)$$

with the relative elongation ϵ caused by magnetostatic interaction parallel to the external magnetic field direction. The elastic modulus of the sample is given by the elastic modulus of the polymer matrix E_{poly} and the volume fraction of the magnetic material φ (with $\varphi \leq 30\%$)^[33,34]

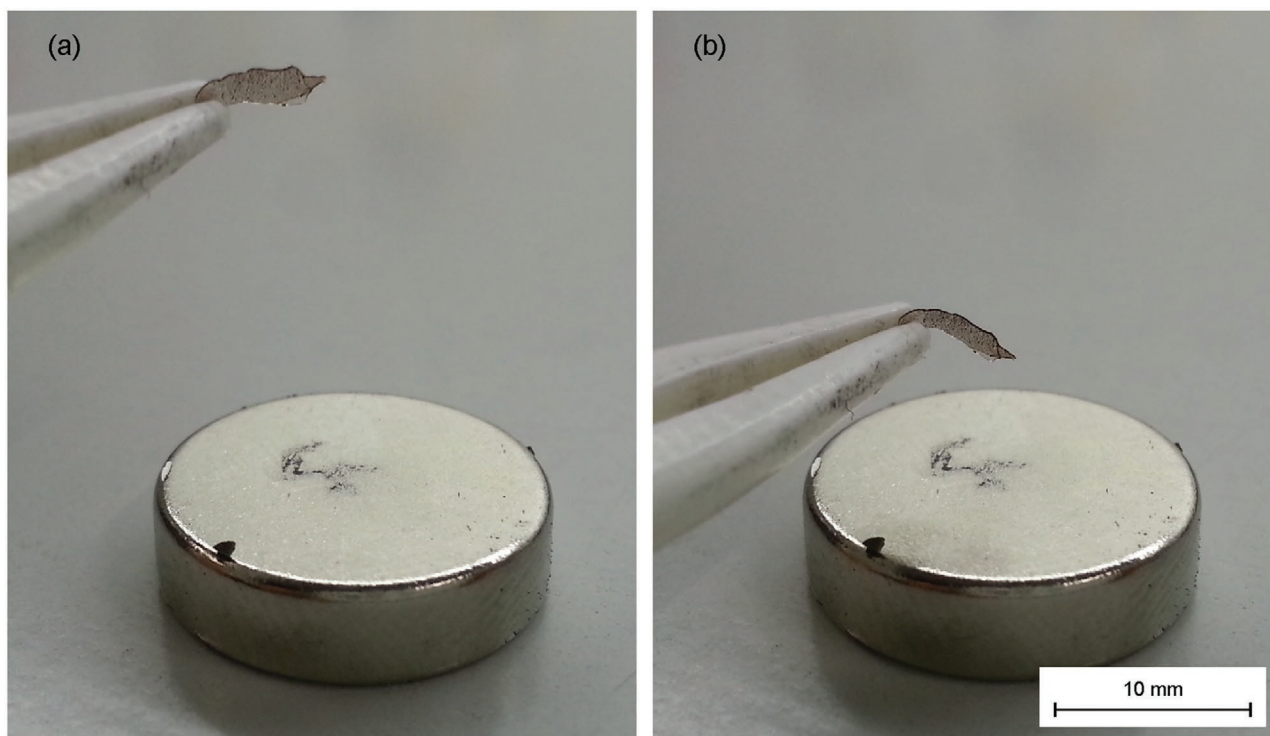


Figure 7. Particle polymer composite type 1 (maghemite particles in PDMS matrix) with 3 wt% of magnetic material (a) and its induced bending motion (b) in spatial proximity to the magnetic field gradient of a Nd permanent magnet (max. 200 mT).

$$E_{\text{sample}} = E_{\text{poly}} (1 + 2.5\phi) \quad (9)$$

Minimizing the total energy of the system by a combination of Equations (1) and (8), the relative elongation ε of the composite when magnetically saturated can be estimated. Therefore, we assume a cylindrical unit cell containing MNP particle agglomerates with diameter d_p in neighboring rows along r_x linked by a PDMS polymer matrix with elastic modulus $E = 1.32 \text{ MPa}$ ^[35] (see Figure 6c). Particle interactions along r_y are neglected at this point since the amount of polymer matrix between the particles is not sufficient to fulfill the condition $\phi \leq 30\%$ and thereby does not provide enough deformable material. For a minimum distance of particle agglomerates to fulfill the mentioned condition, $r_x = 3 \mu\text{m}$, the relative elongation ε results in 6.1% stretching (repulsive interaction) and 8.6% compression (attractive interaction). With the experimental condition of $r_x = 10 \mu\text{m}$, ε is reduced to 0.6% stretching and 0.9% compression.

Due to the fact that the experimentally obtained composites presumably vary from the ideal case assumed in the above estimations considering especially agglomerate shape and behavior, the theoretically predicted elongation could not be observed experimentally. Nevertheless, the overall magnetic responsiveness of the two composite types in inhomogeneous external magnetic fields yielded interesting results despite their extremely low ratio of magnetic material: The films of type 1 with 3 wt% of maghemite visibly react when approaching the magnetic field gradient of a Nd permanent magnet (maximum flux density of 200 mT, see Figure 7), while the particle polymer films of type 2 with superparamagnetic core-shell

particles do not show any reaction to an external magnetic field because of their small amount of magnetic material (0.0014 wt% magnetite) with a magnetic moment determined to be $|\vec{m}| = 4.48 \times 10^{-14} \text{ Am}^2$ ^[36] which is two orders of magnitude lower than the estimated value for a maghemite particle agglomerate.

Additionally, as depicted in Figure 8, it is possible to externally change the spatial position of composite type 1 in water.

Although PDMS itself is hydrophobic, the combination of the gravitational forces due to the additional weight of the magnetic material and the magnetostatic forces between the embedded magnetic particles and the external magnetic field are already strong enough to overcome the repulsive interaction of the PDMS surface and the aqueous environment. As a result, the MNP-PDMS-composite—in contrast to pure PDMS films—can be immersed in water. Considering potential future applications of the magneto-sensitive elastomer, this property seems particularly advantageous as it opens up new opportunities for implementing the biocompatible PDMS.

4. Conclusion and Outlook

We presented a method for a defined positioning of magnetic particles in polymer matrices using magnetically patterned substrate templates. In the current experiments, we introduced magnetically stripe-patterned exchange bias systems as templates for the particles' positioning during the fabrication process of thin particle polymer composites. The positioning process, which is assisted by an additional external magnetic

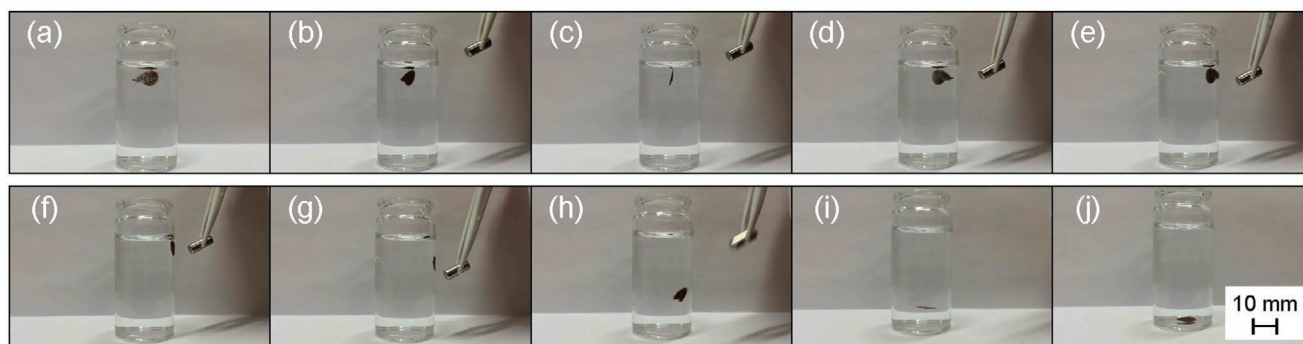


Figure 8. Reaction of particle polymer composite type 1 in water to an external magnetic field generated by a permanent magnet. a) Due to the addition of magnetic material, the hydrophobic PDMS is able to float underneath the water surface. b–d) Approaching the permanent magnet induces a rotation of the composite film. e–g) The composite follows the motion of the permanent magnet. h–j) As soon as the external magnetic field is removed, the composite continues its motion down to the bottom of the flask.

field applied perpendicular to the exchange bias sample plane, works for both Ta and Au capping layers of the exchange bias system as well as for different thicknesses of these layers. The successful anisotropic positioning of magnetic material by utilizing either pure maghemite nanoparticle powder or an aqueous solution of superparamagnetic core–shell microspheres combined with two different polymer types (PDMS and PVOH) indicates that a variety of different materials can be deployed as potential composite components. As stated in previous work, the tailoring of the magnetic stray field landscape and, thereby, the alignment of the magnetic material are not only limited to parallel stripe patterns, but can also be realized into arbitrary 2D geometric shapes, for example, circles.^[22,25] While first investigations confirmed the responsiveness of the composites to external magnetic fields, future studies will focus on the enhancement and on improved controllability of the observed effect. Through further optimization of the respective materials—the shape and strength of the exchange bias system’s magnetic field landscape, the polymer films’ thickness and modulus of elasticity, and the magnitude of the particles’ magnetic moment—the resulting particle polymer composites become highly promising for applications as remotely controllable actuators. This in combination with the proven successful alignment of superparamagnetic microspheres with functionalizable shells opens up the opportunity to implement the composites into medical or biochemical sensor applications.

Acknowledgements

Open access funding enabled and organized by Projekt DEAL.

Conflict of Interest

The authors declare no conflict of interest.

Data Availability Statement

Research data are not shared.

Keywords

exchange bias, ion bombardment, iron oxide, magneto-sensitive elastomers, polydimethylsiloxane, polyvinyl alcohol

Received: April 6, 2021

Revised: October 6, 2021

Published online: October 31, 2021

- [1] J. M. Ginder, M. E. Nichols, L. D. Elie, J. L. Tardiff, in *Smart Structures and Materials 1999: Smart Materials Technologies*, 3675, SPIE, Bellingham, WA 1999, p. 131.
- [2] R. Fuhrer, E. K. Athanassiou, N. A. Luechinger, W. J. Stark, *Small* **2009**, *5*, 383.
- [3] R. L. Snyder, V. Q. Nguyen, R. V. Ramanujan, *Smart Mater. Struct.* **2010**, *19*, 055017.
- [4] H. Böse, R. Rabindranath, J. Ehrlich, *J. Intell. Mater. Syst. Struct.* **2012**, *23*, 989.
- [5] Y. Li, J. Li, W. Li, H. Du, *Smart Mater. Struct.* **2014**, *23*, 123001.
- [6] Z. Rigbi, L. Jilkén, *J. Magn. Magn. Mater.* **1983**, *37*, 267.
- [7] M. R. Jolly, J. D. Carlson, B. C. Muñoz, T. A. Bullions, *J. Intell. Mater. Syst. Struct.* **1996**, *7*, 613.
- [8] L. C. Davis, *J. Appl. Phys.* **1999**, *85*, 3348.
- [9] G. Y. Zhou, Z. Y. Jiang, *Smart Mater. Struct.* **2004**, *13*, 309.
- [10] Z. Varga, G. Filipcsei, M. Zrínyi, *Polymer (Guildf)* **2006**, *47*, 227.
- [11] S. Bednarek, *Appl. Phys. A – Mater. Sci. Process.* **1999**, *68*, 63.
- [12] X. Guan, X. Dong, J. Ou, *J. Magn. Magn. Mater.* **2008**, *320*, 158.
- [13] D. Ivaneyko, V. P. Toshchevnikov, M. Saphiannikova, G. Heinrich, *Macromol. Theory Simul.* **2011**, *20*, 411.
- [14] O. V. Stolbov, Y. L. Raikher, M. Balasoiu, *Soft Matter* **2011**, *7*, 8484.
- [15] W. Chen, L. Sun, X. Li, D. Wang, *Smart Mater. Struct.* **2013**, *22*, 105012.
- [16] T. Gundermann, S. Odenbach, *Smart Mater. Struct.* **2014**, *23*, 105013.
- [17] P. Saxena, J.-P. Pelteret, P. Steinmann, *Eur. J. Mech. A/Solids* **2015**, *50*, 132.
- [18] L. Chen, X. L. Gong, W. H. Li, *Smart Mater. Struct.* **2007**, *16*, 2645.
- [19] T. Tian, M. Nakano, *J. Intell. Mater. Syst. Struct.* **2018**, *29*, 151.
- [20] A. Mougin, S. Poppe, J. Fassbender, B. Hillebrands, G. Faini, U. Ebels, M. Jung, D. Engel, A. Ehresmann, H. Schmoranzler, *J. Appl. Phys.* **2001**, *89*, 6606.
- [21] I. Ennen, V. Höink, A. Weddemann, A. Hütten, J. Schmalhorst, G. Reiss, C. Waltenberg, P. Jutzi, T. Weis, D. Engel, A. Ehresmann, *J. Appl. Phys.* **2007**, *102*, 013910.
- [22] A. Ehresmann, I. Koch, D. Holzinger, *Sensors* **2015**, *15*, 28854.

- [23] A. Mougin, T. Mewes, M. Jung, D. Engel, A. Ehresmann, H. Schmoranzler, J. Fassbender, B. Hillebrands, *Phys. Rev. B* **2001**, 63, 060409.
- [24] A. Ehresmann, D. Engel, T. Weis, A. Schindler, D. Junk, J. Schmalhorst, V. Höink, M. D. Sacher, G. Reiss, *Phys. Status Solidi B* **2006**, 243, 29.
- [25] D. Holzinger, N. Zingsem, I. Koch, A. Gaul, M. Fohler, C. Schmidt, A. Ehresmann, *J. Appl. Phys.* **2013**, 114, 013908.
- [26] N. Zingsem, F. Ahrend, S. Vock, D. Gottlob, *J. Phys. D. Appl. Phys.* **2017**, 50, 495006.
- [27] F. Ahrend, D. Holzinger, M. Fohler, S. Pofahl, U. Wolff, M. DeKieviet, R. Schaefer, A. Ehresmann, *J. Magn. Magn. Mater.* **2015**, 381, 292.
- [28] I. Koch, T. Granath, S. Hess, T. Ueltzhöffer, S. Deumel, C. I. Jauregui Caballero, A. Ehresmann, D. Holzinger, K. Mandel, *Adv. Opt. Mater.* **2018**, 6, 1800133.
- [29] K. L. Pisane, E. C. Despeaux, M. S. Seehra, *J. Magn. Magn. Mater.* **2015**, 384, 148.
- [30] J. Fassbender, S. Poppe, T. Mewes, A. Mougin, B. Hillebrands, D. Engel, M. Jung, A. Ehresmann, H. Schmoranzler, G. Faini, K. J. Kirk, J. N. Chapman, *Phys. Status Solidi* **2002**, 189, 439.
- [31] A. Gaul, D. Emmrich, T. Ueltzhöffer, H. Huckfeldt, H. Doğanay, J. Hackl, M. I. Khan, D. M. Gottlob, G. Hartmann, A. Beyer, D. Holzinger, S. Nemšák, C. M. Schneider, A. Götzhäuser, G. Reiss, A. Ehresmann, *Beilstein J. Nanotechnol.* **2018**, 9, 2968.
- [32] J. Bai, J.-P. Wang, *Appl. Phys. Lett.* **2005**, 87, 152502.
- [33] D. Romeis, P. Metsch, M. Kästner, M. Saphiannikova, *Phys. Rev. E* **2017**, 95, 042501.
- [34] D. Romeis, V. Toshchevikov, M. Saphiannikova, *Soft Matter* **2016**, 12, 9364.
- [35] I. D. Johnston, D. K. McCluskey, C. K. L. Tan, M. C. Tracey, *J. Micro-mech. Microeng.* **2014**, 24, 035017.
- [36] D. Holzinger, I. Koch, S. Burgard, A. Ehresmann, *ACS Nano* **2015**, 9, 7323.